Composite Structures 160 (2017) 538–546

Contents lists available at ScienceDirect

Composite Structures

journal homepage: www.elsevier.com/locate/compstruct

Thickness dependence of mode I interlaminar fracture toughness in a carbon fiber thermosetting composite

Oleksandr G. Kravchenko [a,*], Sergii G. Kravchenko [b], Chin-Teh Sun [b]

[a] Department of Macromolecular Science and Engineering, Case School of Engineering, Case Western Reserve University, 314 Kent Hill Smith Building, Cleveland, OH 44106-7202, United States

[b] School of Aeronautics and Astronautics, Purdue University, 701 W. Stadium Ave., Armstrong Hall of Engineering, West Lafayette, IN 47907, United States

ARTICLE INFO

Article history:
Received 30 March 2016
Revised 16 October 2016
Accepted 21 October 2016
Available online 22 October 2016

Keywords:
K-dominance zone
Fracture process zone
Non-singular opening stress
Apparent fracture toughness

ABSTRACT

The relation of the non-singular opening stress component with apparent fracture toughness was investigated for unidirectional carbon-fiber laminates by means of double cantilever beam experiments in which laminate thickness was varied. It was found that a sample configuration with smaller thickness related to a higher apparent fracture toughness measurement. This result was explained by the presence of a negative non-singular opening stress component, which was found to decrease with thickness. The experimental procedure utilized first crack propagation from the initial polytetrafluoroethylene insert to avoid ambiguity of defining crack location due to crack curving, resulting in a wider crack front and fiber bridging. The two dimensional finite element analyses were used to calculate the corresponding singular and non-singular stress components and the energy release rates. Based on the experimental results a two parameter linear elastic fracture mechanics model was calibrated to incorporate the thickness dependence of the apparent fracture toughness.

1. Introduction

Interlaminar delamination in laminated composites is one of the primary failure mechanisms in different structural components [1]. In general, the development of a crack in a multi-directional laminate leads to a mixed mode fracture condition that is characterized by different crack propagation scenarios [2,3]. The interlaminar delamination subjected to Mode I loading provides the weakest fracture mode in laminated composite materials. The associated value of the fracture toughness in a unidirectional laminate is commonly measured following a standardized test procedure [4]. The standard defines a recommended configuration of a double cantilever beam (DCB) sample [4,5].

From the material characterization point of view it is desirable to have a testing procedure which is easy to conduct and yields consistent data. To ensure that the measured property in a DCB experiment is a true material constant, a great deal of work focused on examining how critical energy release rate, G_{IC}, in thermosetting [6] and thermoplastic composites [7] depends on crack length, sample width [8], sample thickness [8–10] and thickness of the insert [6], as well as displacement rate [11] and load introduction [4]. The standard suggests using a non-adhesive insert, such as a polytetrafluoroethylene (PTFA) film, which works as a crack initiator, yielding consistent results in comparison with pre-cracked samples [6]. The current ASTM standard recommends using the laminate thicknesses in the range of 3–5 mm, since some early experimental results that used compliance calibration methods did not find fracture toughness dependence on the laminate thickness in unidirectional DCB [8–10].

The standard ASTM procedure is concerned with measuring the initiation and propagation values of fracture toughness. A recommended scheme for data reduction is based on a modified beam theory or compliance calibration [4,5], which account for the finite rotation that occurs at the crack front. The recommended approaches suggested by the standard use subsequent crack propagation data from the initial insert. However, with crack propagation initially straight crack front develops curvature due to the anticlastic bending of a plate composing upper and lower halves of a DCB sample [12–14]. Therefore, applying beam model to describe DCB behavior results in the discrepancy between the data reduction scheme and the physical experiment [15].

Curved crack after propagation is a result of a non-uniform distribution of the energy release rate across the sample width during crack initiation [12,14,16]. Not accounting for crack curving in compliance calibration results in an effectively smaller crack

* Corresponding author.
E-mail address: ogkravche@gmail.com (O.G. Kravchenko).

http://dx.doi.org/10.1016/j.compstruct.2016.10.088
0263-8223/

length than when assuming a straight crack front, which will likely result in overestimation of the strain energy release rate [15]. Furthermore, the distribution of G_I across the sample width is a function of sample geometry, and the shape of the curved crack front changes as the crack propagates making the determination of a single crack location ambiguous, due to its curved thumbnail shape [12,13]. Another source of discrepancy introduced with crack propagation is the effect of fiber bridging as a result of fiber migration between the adjacent plies during the early stages of manufacturing [4,17]. Fiber bridging leads to the increase of apparent fracture resistance with subsequent crack propagation from a crack starter (the so called *R*-curve).

In light of these concerns it was the objective of this work to investigate the effects of the laminate thickness on *initiation* critical energy release rates from the straight PTFE insert without using crack propagation data, as opposed to previous experimental studies which included propagation values of G_{IC} using compliance calibration method [8–10]. The 2D finite element analysis of DCB sample allowed to avoid the built-in cantilever boundary condition imposed by the simple beam theory and effectively accommodated finite rotations at the crack front typically accounted by the ASTM recommended data reduction methods. Four groups of DCB samples were tested with thicknesses in the range of 2 mm to 8 mm to obtain the initiation values of G_{IC}. The beam theory and 2D plane strain finite element analysis of DCB samples were used to calculate fracture toughness and yielded a trend of decreasing G_{IC} with increasing laminate thickness. Therefore, a thinner DCB specimen overestimates the fracture resistance of a thicker laminate in terms of the critical energy release rate or stress intensity factor, which are parameters of linear elastic fracture mechanics (LEFM). Only the fracture toughness at crack initiation was measured. To explain the experimentally found differences, the framework of LEFM was used with the emphasis on the K-dominance concept [18–21]. LEFM was shown to work well for materials exhibiting brittle fracture. Such materials are found among engineering plastics and include some thermoplastics as well as thermosetting resins. The incorporation of the *K*-dominance idea into LEFM assumes that fracture toughness for any brittle material is defined not only by the critical value of the stress intensity factor, which describes the *singular* opening stress component [22], but rather the *full* opening stress field, which can differ significantly from the former. The full stress field is described by the Williams series expansion [23], and in addition to the square root singular term it provides higher order terms present in the solution.

The idea of incorporating these higher order terms for better describing the fracture behavior of materials was introduced early by Irwin [22]. Irwin suggested using the first non-singular stress term, constant normal stress in the plane of the crack, denoted later as a *T*-stress, as a second parameter to include the influence of test configurations. This idea was further developed to qualitatively introduce the influence of *T*-stress on the stability of crack propagation direction [24] and the applicability under the assumption of small scale yielding [25,26]. The second non-singular stress component present in the opening stress solution was considered in a similar manner to determine the role of the sample configuration on the apparent fracture toughness in Mode I conditions for polymethyl methacrylate (PMMA) [27,28], which is known to exhibit brittle fracture behavior due to a small fracture process zone [29].

This paper presents the experimental results of fracture toughness testing of DCB with variable thickness of unidirectional thermosetting composite, following the calculation of G_{IC} and using finite element analysis to determine the value of non-singular opening stress. The influence of laminate thickness on *R*-curve was not studied in the present work. The decreasing trend in G_{IC} values with increased thickness of DCB was related to the amplitude of the first non-singular stress component suggesting that it can be used to explain the experimentally found variation of G_{IC} values

2. Materials and testing

The laminates were fabricated from a unidirectional prepreg tape NCT 321 24-700 G150 carbon/epoxy. The laminates were cured in an autoclave following a cure cycle recommended by the manufacturer [30]. A non-adhesive PTFA film (Teflon) was used as a crack initiator [4]. Four unidirectional plates were cured [0_7/Teflon/0_7], [0_{13}/Teflon/0_{13}], [0_{20}/Teflon/0_{20}], and [0_{26}/Teflon/0_{26}] which resulted in thicknesses of 2.03, 4.05, 6.1 and 8.2 mm, respectively. The plates were machined into strips that were used for manufacturing DCB samples of different thicknesses. The schematic of a DCB sample is shown in Fig. 1a. Piano hinges were bonded with paste adhesive to the DCB legs for load introduction as suggested by the ASTM standard [4]. The testing of DCB samples was performed in displacement control in a screw-driven MTS machine for universal mechanical testing. The opening displacement rate was 2 mm/min in all experiments. The linear force-displacement response was observed for all samples up to the maximum load at which crack propagation occurred (shown in Fig. 1b). There was not much variation in the critical force for 2.03, 4.05 and 6.1 mm, but more variation was found for 8.2 mm then for the rest of the samples (Table 1). The crack length measurements were completed by measuring the distance from the end of the PTFA film to the center of the knuckle of the piano-hinge (point of loading).

3. Analysis

3.1. K-dominance at Mode I crack tip in an orthotropic DCB

The fracture of a cracked elastic solid is controlled by the stress/deformation state near the crack tip. Crack driving force is commonly referred to as a parameter which describes the stress/deformation condition at the tip of an existing crack. The crack driving force at crack propagation is defined as critical and is used to quantify the fracture resistance of a material. The region in the vicinity of a crack tip where the inelastic deformation and damage occur is referred to as the fracture process zone (Fig. 2) [29]. The fracture process zone is a microscopic region around the crack tip where material softening develops due to LEFM predicted stresses exceeding the strength of the material as was discussed by Griffith [31]. LEFM assumes that while *the fracture event* occurs in the inelastic region of the fracture process zone, it *is controlled by the deformations in the elastic region surrounding the fracture process zone*.

In the case of Mode I loading, it is generally assumed that the opening stress initiates crack propagation. The stress fields in a linear-elastic body of arbitrary geometry with a sharp crack can be characterized by the asymptotic mathematical solution originally obtained by Williams [23]. According to the Williams series expansion [23], elastic hoop stress distribution, $\sigma_{\theta\theta}$, in the region surrounding the crack tip is given by Eq.(1):

$$\sigma_{\theta\theta}(r,\theta)=\sum_{n=1}^{\infty}A_n r^{\frac{n}{2}-1}f_{\theta\theta}^{(n)}(\theta)=\frac{A_1}{\sqrt{r}}\left[\frac{3}{4}cos\left(\frac{\theta}{2}\right)+\frac{1}{4}cos\left(\frac{3\theta}{2}\right)\right]+2A_2[1-cos(2\theta)]+3A_3\sqrt{r}\left[\frac{5}{4}cos\left(\frac{\theta}{2}\right)-\frac{1}{4}cos\left(\frac{5\theta}{2}\right)\right]+\ldots \quad (1)$$

where (r,θ) are the polar coordinates with their origin at the crack tip (Fig. 2). The coefficients A_n are all proportional to the applied load and further depend on the geometry of the body.

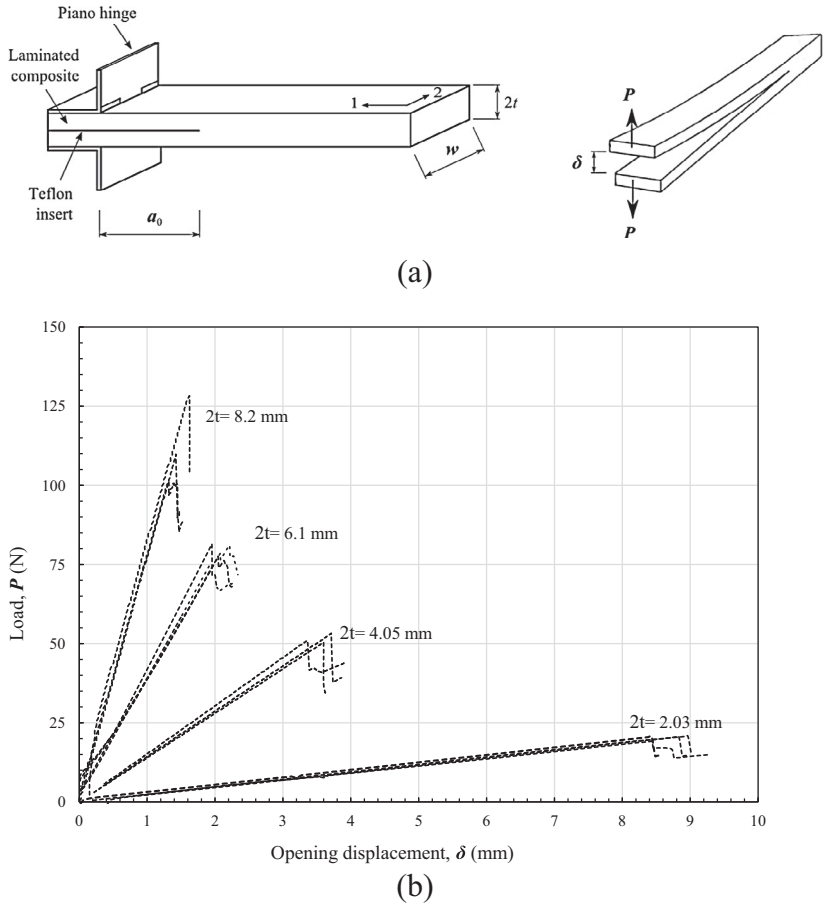

Fig. 1. (a) Schematics of a DCB specimen; (b) load-deflection curves of the DCB samples.

The opening stress, $\sigma_{yy}(x)$, ahead of the crack tip along the crack extension line is

$$\sigma_{yy}(x) = \sigma_{\theta\theta}(r \equiv x,\ \theta = 0) \tag{1a}$$

Table 1
Summary of DCB dimensions and critical force.

Sample #	Force, P_C (N)	Crack length, a (mm)	Width, w (mm)
Laminate thickness, 2t, 2.03 mm (14 plies)			
DCB-2-1	20.560	50.050	19.550
DCB-2-2	20.733	50.050	19.550
DCB-2-3	20.370	50.050	19.550
DCB-2-4	22.200	50.050	19.550
DCB-2-5	19.170	50.160	19.550
Laminate thickness, 2t, 4.05 mm (26 plies)			
DCB-4-1	50.297	50.140	19.600
DCB-4-2	53.308	50.150	19.650
DCB-4-3	50.965	50.100	19.650
DCB-4-4	49.863	50.140	19.650
DCB-4-5	48.832	50.100	19.650
Laminate thickness, 2t, 6.1 mm (40 plies)			
DCB-6-1	80.214	50.370	19.400
DCB-6-2	77.453	50.960	19.400
DCB-6-3	80.426	50.140	19.400
DCB-6-4	77.586	50.450	19.400
DCB-6-5	78.562	49.970	19.500
Laminate thickness, 2t, 8.2 mm (52 plies)			
DCB-8-1	127.00	50.160	19.480
DCB-8-2	101.00	51.925	19.500
DCB-8-3	109.80	51.175	19.500
DCB-8-4	97.593	51.450	19.500

From Eqs. (1) and (1a), the distribution of opening stress can be simplified as

$$\sigma_{yy}(x) = \underbrace{\frac{K_I}{\sqrt{2\pi x}}}_{singular\ \ term} + \underbrace{\sigma(\sqrt{x})}_{Non-singular\ \ terms} \tag{2}$$

where $K_I \equiv A_1\sqrt{2\pi}$ is the Mode I stress intensity factor (SIF). The SIF is defined as:

$$K_I = \lim_{x\to 0}\sqrt{2\pi x}\,\sigma_{yy}(x) \tag{3}$$

The elastic stress field given by Eq. (2) is singular due to the linear formulation of the problem. The singularity suggests that as x approaches zero, the magnitudes of higher order non-singular terms are negligible in comparison with the leading singular term defined by K_I. However, the singular stress term defined by SIF dominates over the rest of the terms in the series only for certain small values of x. The region in the vicinity of the crack tip where the stress is well approximated by the K_I-term alone is referred to as the K-dominance region [18–21]. As x increases, the actual stress $\sigma_{yy}(x)$ is described less and less accurately by retaining only a single K_I-term, because the relative magnitudes of the higher order terms in Eq. (2) begin to contribute increasingly.

Following traditional single-parameter LEFM, the crack driving force is expressed in terms of K_I. In doing so, fracture occurs when the stress intensity, K_I, reaches the critical value, K_{IC}, signifying that the stress distribution ahead of the crack tip becomes substantial (critical) to propagate the crack. LEFM fracture criterion assumes that the K-dominance region extends far enough from the crack tip to confine the fracture process zone and accurately describes

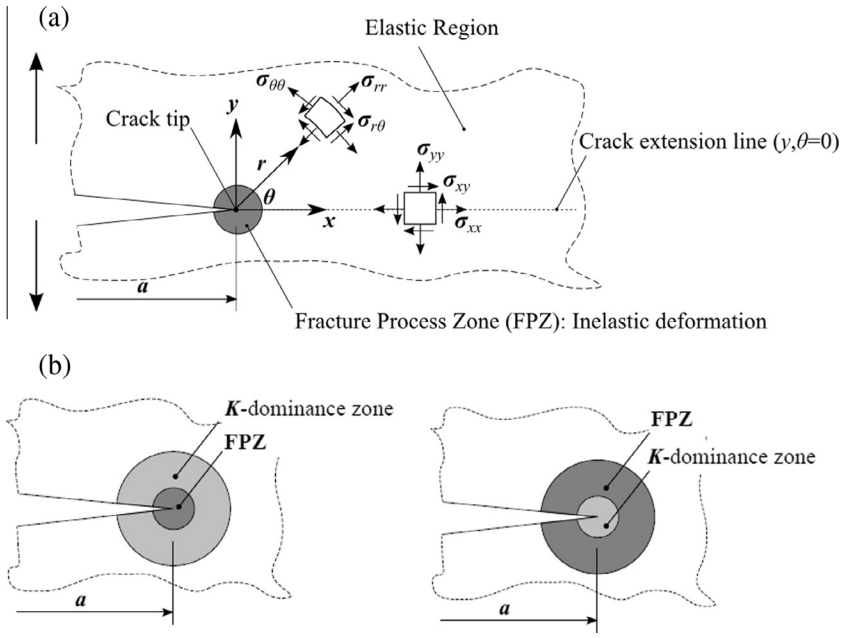

Fig. 2. (a) Coordinate system centered at crack tip; (b) Schematic representation of the *K*-dominance region confining the fracture process zone (on the left) and being confined by the fracture process zone (on the right) (modified from [19]).

the full stress around the fracture process zone, while the fracture event occurs within a fracture process zone. Equivalent to SIF, a single fracture parameter in LEFM is energy release rate (ERR), G_I, which is defined as work per unit area, which is required to create new crack surfaces and given by Eq. (4).

$$G_I = \lim_{\Delta a \to 0} \frac{1}{\Delta a} \int_0^{\Delta a} u_y(x - \Delta a)\sigma_{yy}(x)dx \tag{4}$$

where $u_y(x - \Delta a)$ is the crack opening displacement field obtained from Williams solution at $\theta = \pi$; a is the crack length. If the singular opening stress is used in Eq. (4) it results in the relation between ERR and SIF that relies on the same assumption of the *K*-dominant stress.

The sign and the magnitude of the difference between the opening full stress and *K*-stress depend on the shape of the cracked body. It was first pointed out by Knott [18] that different fracture specimen geometries had varying extensions of *K*-dominance. Let us consider the extent of the region of *K*-dominance in the unidirectional DCB specimens described in Section 2 used for measuring the delamination fracture toughness in unidirectional composite laminates. To investigate *K*-dominance in the finite size specimens, the full opening stress ahead of the crack tip, calculated by means of finite element analysis, was compared with the *K*-stress. Fig. 3 shows the comparison between the full stress and the *K*-based singular stress field in four DCB samples with variable thicknesses used in the experimental work. The full stresses were indicated by the open circles, while singular *K*-stresses were given by the dashed lines. The details of the finite element model used, along with the calculation of K_I and G_I, are provided in Section 3.3. A good agreement between the *K*-field and the full opening stress up to about $x/a = 0.005$ was only seen in the DCB with thickness of $2t = 8.2$ mm. As the DCB thickness decreases, the singular and the full stress profiles differ significantly suggesting that the *K*-stress provided a less accurate approximation of the full stress.

The stresses computed in the finite element analysis, $\sigma_{yy}(x)$, of DCBs were used to calculate the size of the *K*-dominance region. In the current work we defined the region of *K*-dominance in terms of the opening *yy*-component of stress, as this stress component is responsible for Mode I crack propagation. At a given location x, the weight of the singular term in Eq. (2) was quantified by the degree of *K*-dominance [19,20,32], $\Lambda(x)$, defined as

$$\Lambda(x) = \frac{\sigma_{yy}^{(K)}(x)}{\sigma_{yy}^{(K)}(x) + |\sigma_{yy}^{Non-Sing}(x)|} \tag{5}$$

where

$$\begin{aligned} \sigma_{yy}^{(K)}(x) &= \tfrac{K_I}{\sqrt{2\pi x}} \\ \sigma_{yy}^{Non-Sing}(x) &= \sigma_{yy}(x) - \sigma_{yy}^{(K)}(x) \end{aligned} \tag{6}$$

The value of $\Lambda(x)$ can vary from 0 to 1. Analysis of degree of *K*-dominance in four DCB thicknesses is shown in Fig. 4. Near the crack tip there is little deviation between the *K*-stress and the finite element stress, so the value of Λ is close to unity. With increasing distances from the crack tip, the difference between the *K*-field stresses and the actual stresses becomes larger (Λ decreases), thus defining the limit of *K*-dominance. The slope of the K-dominance lines in Fig. 4 scales with laminate thickness. Therefore, the degree of *K*-dominance, $\Lambda(x)$, decreases faster for the thinner DCBs.

In the light of *K*-dominance discussion it becomes important to relate the size of the *K*-dominance to the size of the fracture process zone. The approximate size of the fracture process zone in thermoplastics and toughened thermosetting resins can reach tens of micrometers [29,33]. The distance ahead of the crack tip at which the singular stress, $\sigma_{yy}^{(K)}(x)$, predicts up to 95% of full stress, $\sigma_{yy}(x)$, was used to define the size of the *K*-dominant region. This definition was previously proposed in earlier works on *K*-dominance [21,32]. The size of *K*-dominance is proportional to laminate thickness and the proportionality coefficient was found to be 0.014. Therefore, the size of the *K*-dominance zone varies from 28 to 115 μm for DCB thicknesses from 2.03 to 8.2 mm respectively, which is on the same order of magnitude as the expected fracture process zone size [29,33]. The *K*-dominance zone is small in DCB specimens, suggesting that K_I does not provide a satisfactory approximation of the actual full stress around the fracture process zone at delamination crack tip. Since the *K*-dominance depends heavily on a DCB thickness, it makes the critical crack

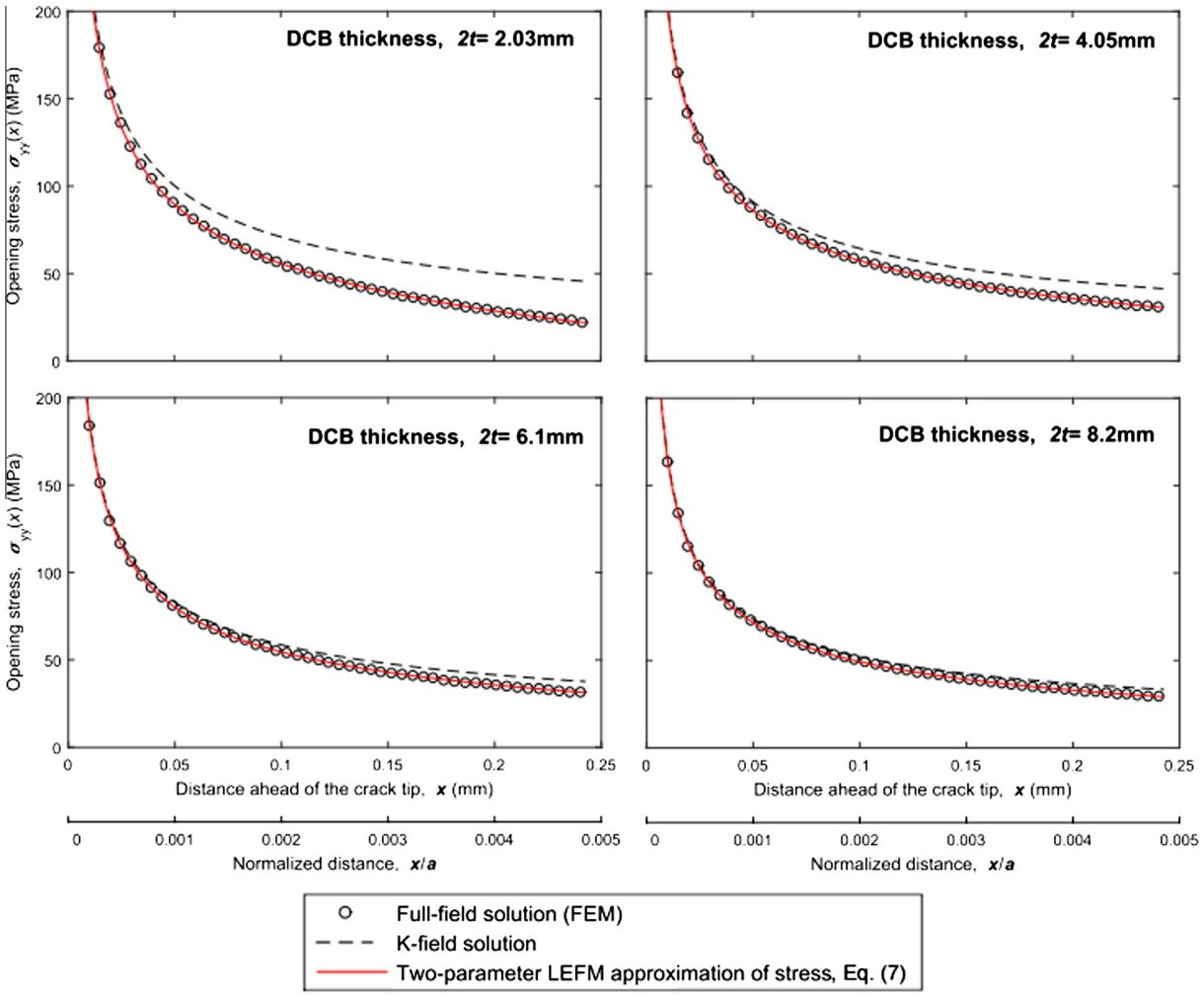

Fig. 3. Full and singular opening stress profiles in DCB samples.

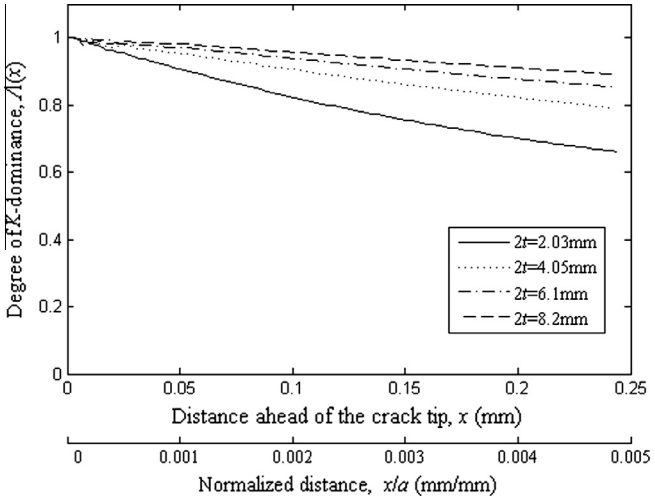

Fig. 4. Degree of K-dominance in DCB specimens of variable thickness.

driving force, expressed in terms of SIF, dependent on the specimen geometry. Consequently, the dependence of measured interlaminar fracture toughness on the test piece geometry undermines the principle of a single parameter LEFM and is commonly referred to as constraint effect [27,28,34]. The constraint effect creates a problem for the transferability between the fracture toughness measured using a sample configuration and the full-scale engineering structure, which may have a different constraint level. The way to incorporate the constraint effect is by including the higher (non-singular) terms to the formulation of the crack driving force [27,28,32]. The connection between the amplitude of non-singular opening stress and the apparent delamination fracture toughness is discussed in the following sections.

3.2. Quantification of non-singular opening stress

Assume that the approximation of the stress profile ahead of the crack tip with singular and non-singular components is given by Eq. (7):

$$\sigma_{yy}(x) \cong \frac{K_I}{\sqrt{2\pi x}} + 3A_3\sqrt{x} \tag{7}$$

The form of Eq. (7) corresponds to using the first non-singular term from William's series expansion. Eq. (7) provides a good approximation of the full opening stress obtained with FEM over an extended region of x as it can be seen from Fig. 3. The role of the non-singular opening stress term is that it allows for incorporation of the finite boundaries of the sample and its effect on the stress distribution around the crack tip. Thus, it has a similar role as a constant T-stress as was first suggested by Irwin [22]. The magnitude as well as the sign of the non-singular opening stress component can be different for different specimen configurations, as was previously discussed in Refs. [21,34,20,19].

It appears that for common DCB specimen geometries the first non-singular opening stress term is negative (compressive). The first (singular) term is always positive in opening Mode I condition, and as a result the full opening stress in front of the crack tip is less than the stress predicted by SIF alone. When $|A_3|$ is small the deviation of the stress from the K-stress is small (Fig. 3). While deviation is negligible, a large region around the crack tip is dominated by the first term in Eq. (7). Hence, a single parameter K_I can be used as a measure of stress to characterize the onset of crack propagation. When $|A_3|$ is large the full opening stress deviates substantially from the K-stress. Therefore, the concept of using a single parameter to characterize the onset of fracture initiation becomes doubtful. By multiplying both sides in Eq. (7) with $\sqrt{2\pi x}$ the following expression is obtained:

$$\sigma_{yy}\sqrt{2\pi x} = K_I + 3\sqrt{2\pi}A_3 x = K_I + Cx \tag{8}$$

where $C = 3\sqrt{2\pi}A_3$ is referred to as the amplitude of non-singular stress.

To further evaluate the relative magnitudes of the non-singular opening stress profiles the expression (8) was normalized by SIF:

$$\sigma_{yy}\frac{\sqrt{2\pi x}}{K_I} = 1 + \bar{C}x \tag{9}$$

where $\bar{C} = C/K_I$ normalized amplitude of non-singular opening stress.

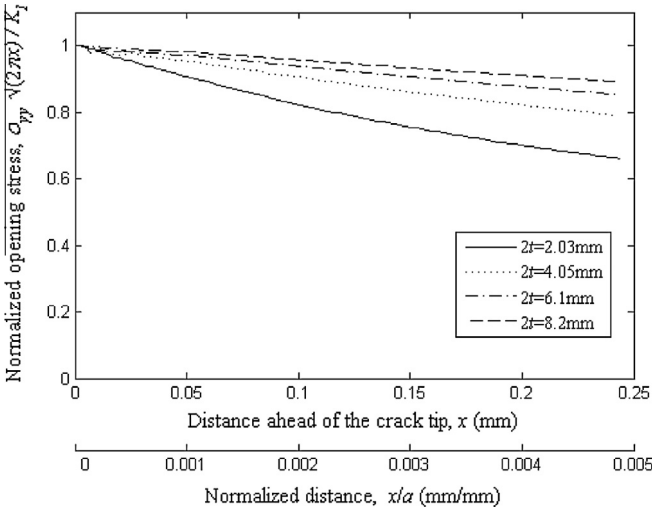

Fig. 5. Normalized opening stress distribution away from the crack tip.

The finite element solution for each of the four DCB thicknesses was used to investigate the left hand side of Eq. (9) (shown in Fig. 5). At the crack tip the numerical solution diverges due to the stress singularity; however, away from crack tip, the left hand side of Eq. (8) follows a linear behavior. Because of negative slope of lines in Fig. 5, it can be concluded that the non-singular opening stress term is compressive for all of the DCB thicknesses considered and that absolute value of its amplitude increases as thickness of DCB becomes smaller.

3.3. Finite element based calculation of ERR and SIF

In the present work two dimensional plane-strain analyses were used to calculate ERR and SIF. The finite element mesh was refined around the crack tip with the element size of 2.5 μm (shown in Fig. 6) to ensure stress convergence around the crack tip. Large deflection analysis was used.

The material properties of the unidirectional composite used for the analysis are given in Table 2. For a homogeneous linear elastic solid both ERR and SIF are equivalent for prescribing the critical condition of crack propagation. In the case of an orthotropic material the expressions relating ERR to SIF are given by the following [35]:

$$G_I = b_{11}n\lambda^{-3/4}K_I^2 \tag{10}$$

where λ and n are non-dimensional elastic parameters given by the following

$$\lambda = \frac{b_{11}}{b_{22}} \tag{11}$$

$$n = \left(b_{12} + \frac{1}{2}b_{66}\right)(b_{11}b_{22})^{-0.5} \tag{12}$$

and

$$b_{ij} = \begin{cases} s_{ij} & \text{(plane stress)} \\ s_{ij} - s_{i3}s_{j3}/s_{33} & \text{(plane strain)} \end{cases} \tag{13}$$

where $i,j = 1, 2, 6$; s_{ij} are elastic compliances.

Finite element analysis can be used to determine the critical energy release rate using one of the available techniques [19,35,36]. In this work, modified virtual crack closure technique [37] (VCCT) was used to calculate G_{IC}. The critical force from each experiment was used to find the corresponding G_{IC}. For a four-node plane strain elements, calculation based on modified VCCT used the following equation to find G_{IC}

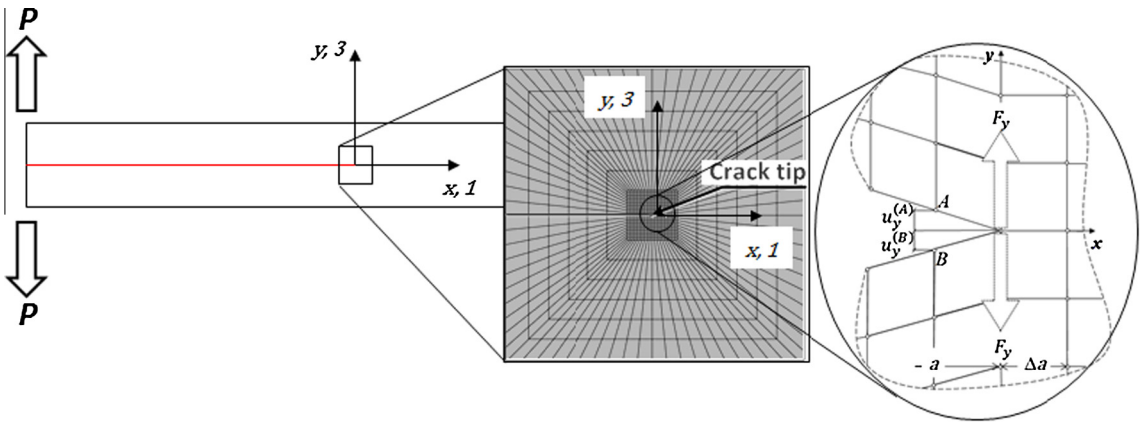

Fig. 6. Schematics of finite element model around the crack tip with parameters for VCCT calculation.

Table 2
Mechanical properties of NCT 321 34-700 G150.

Laminate NCT 321 34-700 G150	
Mechanical constant (Units)	Magnitude
Longitudinal Young's modulus, E_1 (GPa)	110.00
Transverse Young's modulus, E_2, E_3 (GPa)	8.066
Shear moduli, G_{12}, G_{13} (GPa)	3.790
Shear modulus, G_{23} (GPa)	3.280
Poisson's ratios, ν_{12}, ν_{13}	0.321
Poisson's ratio, ν_{23}	0.45

$$G_I = \frac{1}{2\Delta a} F_y (u_y^{(A)} - u_y^{(B)}) \tag{14}$$

where F_y is a reactive force per unit width calculated from the stress adjacent to the crack tip node elements and $u_y^{(u)}, u_y^{(l)}$ are the vertical displacement terms of the upper and lower nodes at the crack tip; Δa is the mesh size at the crack tip (Fig. 6).

Projection method is based on the calculation of stress intensity factor, K_I, using the opening stress distribution ahead of the crack tip from finite element solution. When plotting $\sigma_{yy}\sqrt{2\pi x}$ (Fig. 7) as a function of distance x from the crack tip, the resulting curve is a straight line of slope $C = 3\sqrt{2\pi}A_3$, Eq. (8), close to the crack tip where the higher order terms are small. The intersection of the line with the ordinate axis provides the numerical value of the stress intensity factor, following the definition of SIF given by Eq. (3).

4. Experimental findings and interpretation of results

4.1. Calculation of a single critical fracture parameter from experimental results

Mode I interlaminar fracture toughness of the laminate was measured in terms of the critical values of energy release rate (ERR), G_{IC}, and stress intensity factor (SIF), K_{IC}. Both of these parameters, ERR and SIF, are conventionally used to represent the driving force of an existing crack, when one-parameter fracture mechanics is used to describe fracture.

Values of critical ERR were calculated by beam theory given in Eq. (15). The ASTM D 5528 [4] recommended methods (modified beam theory, compliance calibration, or modified compliance calibration) were not used herein since they required sequential crack extension measurements from the initial pre-crack (Teflon insert), which was beyond the scope of the current work to avoid the aforementioned complications associated with crack curving and fiber bridging. Therefore, the authors were interested in the initiation values of delamination fracture toughness.

$$G_{IC} = \frac{3}{2}\frac{P_c \delta_c}{wa} \tag{15}$$

where P_c and δ_c are critical force and displacement at crack initiation.

The results of ERR calculation using beam theory are shown in Fig. 8. Furthermore, the values of G_{IC} were also calculated by modified VCCT and by the projection method. It was found that the results by VCCT and projection methods agree within 0.7–1.8%, confirming that both techniques were applicable for calculating energy release rate. The beam theory produces consistently higher values than from finite element analysis due to the assumptions of the cantilever beam (Figs. 8 and 9) [4].

4.2. Variation of apparent interlaminar fracture toughness with laminate thickness

Apparent Mode I delamination fracture toughness when measured in terms of ERR or SIF was found to depend on the laminate thickness. Thicker double-cantilever beam (DCB) specimens were found to exhibit lower apparent fracture toughness than their thinner counterparts in terms of conventional single linear-elastic fracture mechanics parameters such as critical stress intensity factor, K_{IC}, and energy release rate, G_{IC}, as shown in

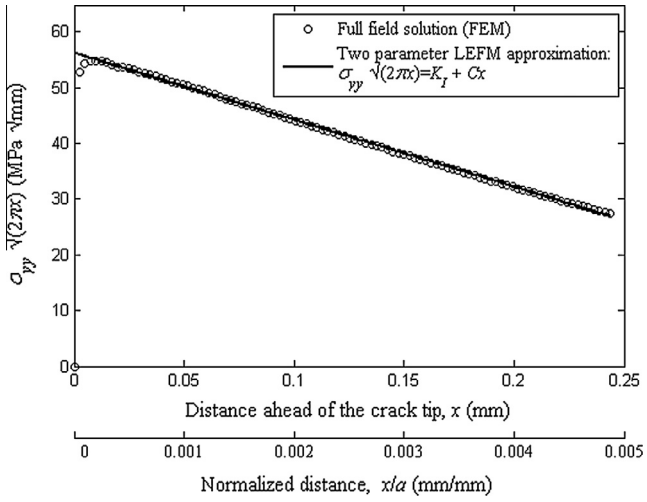

Fig. 7. Projection method to calculate K_I (data corresponds to 2.03 mm thick DCB specimen).

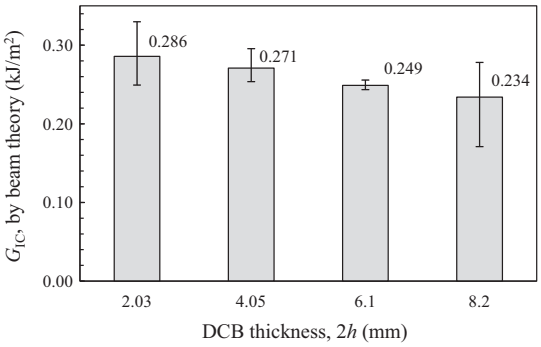

Fig. 8. Experimental results of G_{IC} with different DCB thicknesses calculated by beam theory.

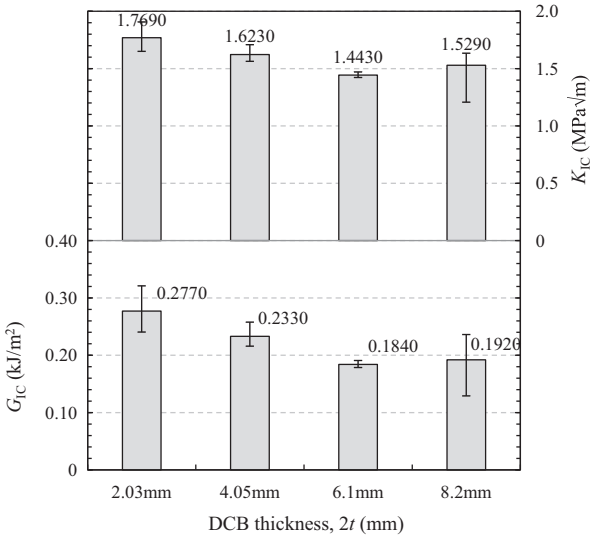

Fig. 9. Experimental results of G_{IC} with different DCB thicknesses calculated by FEA.

Fig. 9. Some scatter of the experimental data within same DCB thickness was observed, which is usual in the fracture toughness experiments of composites [2,38]. While some of the test results of G_{IC} for different thicknesses showed overlap (2.03 and 4.05 mm), no overlap was found between DCB thicknesses of 2.03 and 6.1 mm and between 2.03 and 8.2 mm. By considering the average values and using 2.03 mm-thick DCB as a reference, the difference between DCB with 2.03 and 4.05 mm thickness was about 16%, while the difference for DCB with thickness of 2.03 and 8.2 mm was 32%. This observation contradicts the widely accepted assumption that the results of the DCB experiment present a fracture toughness material constant that is independent of the sample geometrical configuration. The experimentally observed differences in the first crack propagation values of G_{IC} cannot be explained simply by the experimental scatter, nor by the differences in the microstructure mechanical properties or residual cure stresses, since all laminates were cured following an identical cure cycle.

For a DCB configuration of smaller thickness, the size of the K-dominance zone is small or on the same order of magnitude with the fracture process zone. Therefore SIF alone overestimates the opening stress at the crack tip because of the compressive non-singular opening stress which is overlooked by the single parameter LEFM. Consequently, this results in higher apparent interlaminar fracture toughness. In other words, higher apparent fracture toughness would be obtained from test specimens, which had a larger absolute value of negative non-singular term, $|A_3|$. The correlation between the apparent SIF, K_I, and the amplitude of the non-singular opening stress, $C = 3\sqrt{2\pi}A_3$, calculated at crack propagation is seen from Fig. 10. Consequently, the presence of the large compressive non-singular stress component in thinner DCB samples was responsible for higher apparent critical SIF/ERR, K_{IC}/G_{IC}, measurements determined experimentally. Since the opening stress ahead of the crack tip was shown to be approximated by two parameters K_I and A_3 with improved accuracy, it would be quite natural to use both of them to define the crack driving force for characterizing the onset of fracture. The critical SIF or ERR alone would provide a true material property for fracture toughness only if there was a specimen geometry with A_3 close to zero. This finding confirms the similar results for PMMA reported previously both in static and fatigue loading [28,32,34].

4.3. Two parameter fracture mechanics model of apparent interlaminar fracture toughness

A two-parameter LEFM model to characterize fracture event is developed in the present section. For engineering purpose it is convenient to relate the amplitude of non-singular stress, C, which is apparent to the particular geometry (laminate thickness), to the critical SIF, K_{IC}^{ap}. Thus, a combination of these two parameters (K_{IC}^{ap}, C) represents a critical crack driving force at the tip of an existing delamination crack. Let us assume that the fracture event onset under Mode I is controlled by the critical opening stress (7) distribution defined over some finite critical distance, x_c, ahead of the crack tip. At a finite distance x from the crack tip, the stress is described more accurately when higher order (non-singular) terms are retained along with the first singular term. However, the fracture process should remain unique whether only a singular stress or both singular and non-singular stresses are involved. The following condition was expressed by Eq. (15) and allowed the equivalence of the resultant opening force over the critical distance in the case when non-singular stress is zero and when a pair of K_I^{ap} and C are used to describe the full stress:

$$\int_0^{x_c} \frac{K_{IC}^{(0)}}{\sqrt{2\pi x}} dx = \int_0^{x_c} \left(\frac{K_{IC}^{ap}}{\sqrt{2\pi x}} + 3A_3\sqrt{x} \right) dx \tag{16}$$

where $K_{IC}^{(0)}$ is the critical SIF corresponding to non-singular opening stress being zero (an "ideal" very thick DCB specimen); (K_{IC}^{ap}, A_3) are the apparent SIF and non-singular terms defining the fracture condition for a given laminate thickness.

After simplification Eq. (16), the apparent critical SIF depends on the level of non-singular stress, C, as given by Eq. (17):

$$K_{IC}^{ap} = K_{IC}^{(0)} - \sqrt{2\pi}A_3 x_c = K_{IC}^{(0)} - \frac{x_c}{3} C \tag{17}$$

$K_{IC}^{(0)}$ and x_c are the material parameters which must be determined from the experimentally found combinations (K_{IC}^{ap}, C) at fracture. The fracture curve based on the least-squares fit and the experimental data are depicted in Fig. 10. From the curve fit it was evaluated that $K_{IC}^{(0)} = 45.0\ \text{MPa}\sqrt{\text{mm}}$ and $x_c = 0.28$ mm for a considered carbon/epoxy material system.

Further, when necessary, the critical ERR, G_{IC}, apparent to the given laminate thickness can be estimated from the SIF, K_{IC}, by Eq. (10). The importance of using the appropriate value of apparent material fracture toughness can be illustrated by the following. The interlaminar fracture toughness is used in modeling of progressive damage in composite materials by incorporating it in a progressive damage model or cohesive zone law. As it was discussed in the present work, the delamination resistance depends on the geometry and the loading conditions of the laminated composite. To correctly describe the delamination propagation scenarios in laminated composites, the apparent fracture toughness must be

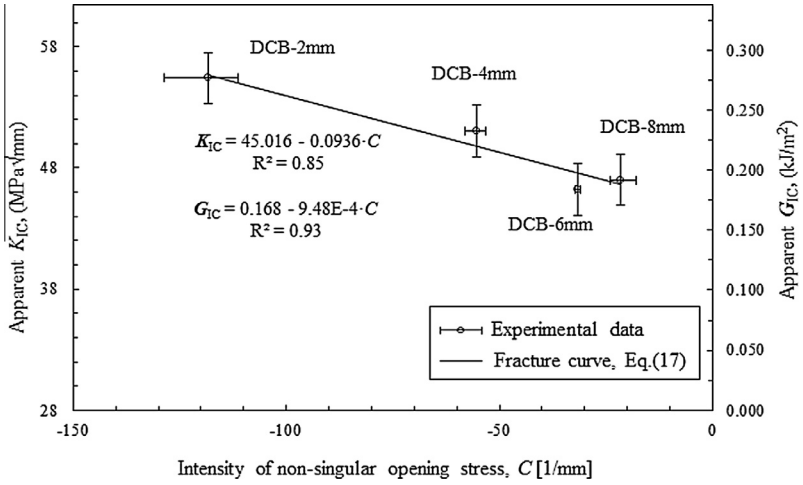

Fig. 10. Dependence of the apparent G_{IC} on the intensity of the non-singular opening stress.

included in the cohesive model based on the results of the linear elastic analysis. The linear analysis allows calculating the amplitude of the non-singular opening stress and the corresponding apparent interlaminar fracture toughness that can be used in the definition of the cohesive law.

5. Conclusions

The thickness dependence of the apparent delamination fracture toughness in laminated unidirectional composites was investigated using DCB specimens of different thicknesses. To avoid the associated discrepancy in the experiment due to crack curving after initial crack propagation from the Teflon film insert and fiber bridging, only the first (initiation) values of fracture toughness were considered. Higher fracture toughness values were found for thinner DCB specimen. To explain such phenomenon, a linear elastic solution was examined to include the second non-singular opening stress component by means of 2D plane-strain finite element analysis. The size of the *K*-dominant zone was found to be on the same order of magnitude as the sizes of the fracture process zones reported in the literature for the brittle thermosets and thermoplastics. In such a case, the role of the non-singular stress component becomes important. It was found that for the considered DCB thicknesses, the non-singular opening stress component was negative, and its relative magnitude with respect to the singular stress was higher in thinner DCB samples. The amplitude of non-singular opening stress was calculated from FEA analysis and related to the apparent fracture toughness.

The classical LEFM predicts the local fracture event using a single parameter, which describes singular stresses at the crack tip. However, a single parameter criterion provides an incomplete description of the near crack tip stress conditions in the case of interlaminar fracture toughness testing with the DCB specimen configuration. The critical ERR or SIF depend on the structural constraint (thickness) of a DCB test sample, so the single parameter fails to precisely describe the actual full stress field at the vicinity of a crack tip and should be used carefully in order to characterize the fracture behavior of the material. Ignoring the constraint effects can result in a transferability problem of the delamination toughness measured on a laboratory specimen and the integrity assessment of a damage tolerant laminated composite structure. The basic requirement for transferability is that the critical values of the parameters used to characterize singular and non-singular stress components must be the same in a tested specimen and in the actual structural component.

References

[1] Sela N, Ishai O. Interlaminar fracture toughness and toughening of laminated composite materials: a review. Composites 1989;20:423–35.
[2] Hwu C, Kao CJ, Chang LE. Delamination fracture criteria for composite laminates. J Compos Mater 1995;29:1962–87.
[3] Nicholls DJ, Gallagher JP. Determination of GIC in angle ply composites using a cantilever beam test method. J Reinf Plast Compos 1983;2:2–17.
[4] ASTM D5528-13. Standard test method for Mode I interlaminar fracture toughness of unidirectional fiber-reinforced polymer matrix composites. West Conshohocken, PA: ASTM International; 2013. www.astm.org.
[5] Berry JP. Determination of fracture surface energies by the cleavage technique. J Appl Phys 1963;34:62–8.
[6] Davies P, Moulin C, Kausch HH, Fischer M. Measurement of GIc and GIIc in carbon/epoxy composites. Compos Sci Technol 1990;39:193–205.
[7] Davies P, Cantwell W, Moulin C, Kausch HH. A study of the delamination resistance of IM6/PEEK composites. Compos Sci Technol 1989;36:153–66.
[8] Davies P, Kausch HH, Williams JG, Kinloch AJ, Charalambides MN, Pavan A, Moore DR, Prediger R, Robinson I, Burgoyne N, Friedrich K, Wittich H, Rebelo CA, Torres Marques A, Ramsteiner F, Melve B, Fischer M, Roux N, Martin D, Czarnocki P, Neville D, Verpoest I, Goffaux B, Lee R, Walls K, Trigwell N, Partridge IK, Jaussaud J, Andersen S, Giraud Y, Hale G, McGrath G. Round-robin interlaminar fracture testing of carbon-fibre-reinforced epoxy and PEEK composites. Compos Sci Technol 1992;43:129–36.
[9] Prel YJ, Davies P, Benzeggagh ML, de Charentenay F-X. Mode I and Mode II delamination of thermosetting and thermoplastic composites. Compos Mater: Fatigue Fract, 2; 1989.
[10] Hojo M, Aoki T. Thickness effect of double cantilever beam specimen on interlaminar fracture toughness of AS4/PEEK and T800/epoxy laminates. Compos Mater Fatigue Fract, 4; 1993.
[11] Hashemi S, Kinloch AJ, Williams JG. The effects of geometry, rate and temperature on the Mode I, Mode II and mixed-Mode I/II interlaminar fracture of carbon-fibre/poly(ether-ether ketone) composites. J Compos Mater 1990;24:918–56.
[12] Davidson BD. An analytical investigation of delamination front curvature in double cantilever beam specimens. J Compos Mater 1990;24:1124–37.
[13] Davidson BD, Schapery RA. Effect of finite width on deflection and energy release rate of an orthotropic double cantilever specimen. J Compos Mater 1988;22:640–56.
[14] Nilsson K-F. On growth of crack fronts in the DCB-test. Compos Eng 1993;3:527–46.
[15] Sun CT, Zheng S. Delamination characteristics of double-cantilever beam and end-notched flexure composite specimens. Compos Sci Technol 1996;56:451–9.
[16] Kravchenko O. Effect of specimen dimensions on interlaminar fracture toughness of composites (MS thesis). Purdue University; 2012.
[17] Hashemi S, Kinloch AJ, Williams JG. Mechanics and mechanisms of delamination in a poly(ether sulphone)—fibre composite. Compos Sci Technol 1990;37:429–62.
[18] Knott JF. Fundamentals of fracture mechanics. Gruppo Italiano Frattura; 1973.
[19] Bratschi B. Modeling brittle constrained fracture with cohesive zone models (Ph.D. thesis). Purdue University; 2014.
[20] Sun C-T, Jin Z. Fracture mechanics. Academic Press; 2011.
[21] Becker Jr TL, McNaney JM, Cannon RM, Ritchie RO. Limitations on the use of the mixed-mode delaminating beam test specimen: effects of the size of the region of K-dominance. Mech Mater 1997;25:291–308.
[22] Irwin GR. Analysis of Stresses and strains near the end of a crack traversing a plate. J Appl Mech 1957;24:361–4.
[23] Williams ML. On the stress distribution at the base of a stationary crack. J Appl Mech 1957;24:361–4.
[24] Cotterell B. Notes on the paths and stability of cracks. Int J Fract Mech Sep. 1966;2:526–33.
[25] Larsson SG, Carlsson AJ. Influence of non-singular stress terms and specimen geometry on small-scale yielding at crack tips in elastic-plastic materials. J Mech Phys Solids 1973;21:263–77.
[26] Rice JR. Limitations to the small scale yielding approximation for crack tip plasticity. J Mech Phys Solids Jan. 1974;22:17–26.
[27] Chao YJ, Liu S, Broviak BJ. Brittle fracture: variation of fracture toughness with constraint and crack curving under Mode I conditions. Exp Mech Sep. 2001;41:232–41.
[28] Kravchenko SG, Kravchenko OG, Sun CT. A two-parameter fracture mechanics model for fatigue crack growth in brittle materials. Eng Fract Mech Mar. 2014;119:132–47.
[29] Williams JG. Fracture mechanics of polymers. New York: Halsted Press; 1985.
[30] Newport 321 Product Data Sheet, Newport Adhesives and Composites Inc, Mitsubishi Rayon Group; 2006.
[31] Griffith AA. The Phenomena of Rupture and Flow in Solids. Philosophical Transactions of the Royal Society of London. Series A, Containing Papers of a Mathematical or Physical Character, vol. 221, 1921, p. 163–198.
[32] Kumar B, Chitsiriphanit S, Sun CT. Significance of K-dominance zone size and nonsingular stress field in brittle fracture. Eng Fract Mech 2011;78:2042–51.
[33] Sue H-J. Craze-like damage in a core-shell rubber-modified epoxy system. J Mater Sci 1992;27:3098–107.
[34] Chao YJ, Yang S, Sutton MA. On the fracture of solids characterized by one or two parameters: theory and practice. J Mech Phys Solids 1994;42:629–47.
[35] Hutchinson JW, Suo Z. Mixed mode cracking in layered materials. Adv Appl Mech 1991;29:63–191.
[36] Banks-Sills L. Application of the finite element method to linear elastic fracture mechanics. Appl Mech Rev 1991;44:447–61.
[37] Rybicki EF, Kanninen MF. A finite element calculation of stress intensity factors by a modified crack closure integral. Eng Fract Mech 1977;9:931–8.
[38] Ozdil F, Carlsson LA. Beam analysis of angle-ply laminate DCB specimens. Compos Sci Technol 1999;59:305–15.